Pertanika J. Sci. & Technol. 26 (2): 585 - 598 (2018)

SCIENCE & TECHNOLOGY

Journal homepage: http://www.pertanika.upm.edu.my/

Demonstration of Comparison between Goat Skin and X-Ray Film Membranes on Traditional Musical Instrument Kompang

W. A. Siswanto[1] and M. Syiddiq[2]*

[1]*Department of Mechanical Engineering, Universitas Muhammadiyah Surakarta (UMS), Surakarta 57102, Indonesia*

[2]*Department of Engineering Mechanics, Universiti Tun Hussein Onn Malaysia, 86400 UTHM, Batu Pahat, Johor, Malaysia*

ABSTRACT

This paper presents a mathematical model of the traditional musical instrument, the *kompang*. In this study, a mathematical model of the *kompang* membrane is developed to simulate the vibration of the *kompang* membrane in polar coordinates by implementing the Fourier-Bessel wave function. The wave equation in polar direction is applied to provide the vibration modes of the membrane with the corresponding natural frequencies of the circular membrane. The initial and boundary conditions are determined to allow the development of numerical equation based on *kompang* membrane attachment. The mathematical model is coded in Smath for the numerical analysis as well as the plotting tool. Two *kompang* membrane cases with different membrane materials i.e. goat-skin and x-ray film are tried to test the model. The Finite Element Method (FEM) programme, Mecway, shows that the natural frequencies and the corresponding mode shapes are comparable with those from the developed model.

Keywords: Fourier-Bessel function, kompang, musical instrument modelling

INTRODUCTION

Specific traditional musical instruments and percussion instruments have been investigated and their mathematical models have been found to represent their vibration characteristics. Several tests and numerical studies have been performed in this area. Christian et al. (1984) and Rhaouti et al. (1999) reported on kettledrums, while Bertsch (2001), and Bilbao and Webb (2012) documented data on timpani. Research into musical instruments has also been done by Rossing et al. (1992) and Bilbao (2012), who did work on snare drums. Siswanto et al. (2014) reported on traditional musical instruments, providing documentation on the reproduction of the *kompang* sound and details of their analysis of the sound of the *kompang* for computer music synthesis (Ismail et al., 2006).

Article history:
Received: 2 January 2017
Accepted: 11 January 2018

E-mail addresses:
waluyo@ums.ac.id (W. A. Siswanto)
cdix91@gmail.com (M. Syiddiq)
*Corresponding Author

ISSN: 0128-7680 © 2018 Universiti Putra Malaysia Press.

In this paper, the traditional percussion instrument, the *kompang*, that was used was from Johor, Malaysia. The musical instrument consists of two interacting components: a membrane and a rigid shell used for holding the membrane (See Figure 1). During *kompang* making, it is important to install the membrane to the *kompang* wood shell correctly and firmly. Incorrect installment of the membrane to the shell generates non-uniform movement across the membrane, causing inconsistency in terms of the sound (Ono et al., 2009). The *kompang* comes in various sizes, normally with a radius between 22 cm and 35 cm and a frame height between 4 cm and 6 cm (Abdullah, 2005). Continuous rigorous hitting of the membrane of the *kompang* usually can cause displacement of the *kompang* by several millimetres, that is a displacement that can be greater than the thickness of the membrane itself. It is reasonable to expect that different membranes have different sound attributes (Bank & Sujbert, 2006).

This paper aimed to provide a clear understanding of the traditional percussion musical instrument, the *kompang*, through a mathematical model of the instrument from a computational perspective. An understanding of traditional musical instruments is crucial as these instruments represent the cultural values of its users, as pointed out by Karjalainen et al. (1993), who studied the traditional musical instrument of Finland, the *kantele*. This study focusses on traditional musical instrument *kompang* for Malaysian region. In this paper, two types of *kompang* are considered: a goat-skin membrane *kompang* (see Figure 1) and an x-ray film membrane *kompang* (see Figure 2).



Figure 1. The traditional musical instrument, the *kompang*, using goat-skin for the membrane



Figure 2. The traditional musical instrument, the *kompang*, using x-ray film for the membrane

MATHEMATICAL DEVELOPMENT

Displacement of the circular membrane of the *kompang* during playing is due to the applied force from hitting the membrane of the instrument. The magnitude of the displacement depends on the radius of the circular membrane. Polar coordinates were selected in this study since the *kompang* membrane is circular in shape.

Forces on the *Kompang* Membrane

The forces exacted on the displaced membrane can be identified from the general mathematical equation of the membrane in polar coordinates as implemented by Morse (1948).

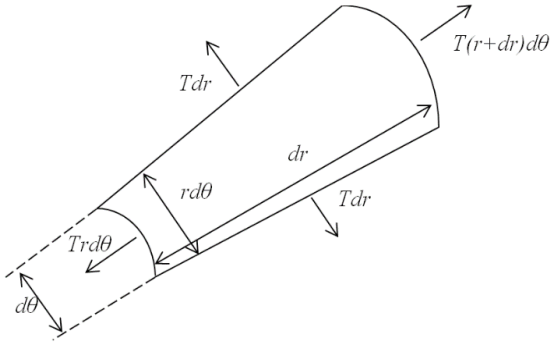

Figure 3. Forces on an element of a membrane in polar coordinates

Let us consider Figure 3. The net force due to the tensions perpendicular to the radius are given as:

$$Tdr\left[\left(\frac{\partial u}{r\partial\theta}\right)_{\theta+\partial\theta}-\left(\frac{\partial u}{r\partial\theta}\right)_{\theta}\right]=\frac{T}{r^2}\frac{\partial^2 u}{\partial\theta^2}rdrd\theta \quad (1)$$

where, r is the radius of the membrane, T is the tension of the membrane per length and θ is the angle around the axis of the membrane.

Due to the tensions parallel to the radius, the following equation is derived:

$$Td\theta\left[\left(r\frac{\partial u}{\partial r}\right)_{r+\partial r}-\left(r\frac{\partial u}{\partial r}\right)_{r}\right]=\frac{T}{r}\frac{\partial}{\partial r}\left(r\frac{\partial u}{\partial r}\right)rdrd\theta \quad (2)$$

The Laplacian Operator

Laplacian operator is denoted by ∇^2, which can be applied in the operation to find a bulge point along the membrane surface, u, at some point (Morse, 1948). Applying the wave equation properties, we have:

$$\nabla^2 u=\frac{1}{c^2}\frac{\partial^2 u}{\partial t^2} \quad (3)$$

The equation of motion in polar coordinates at a point is:

$$\frac{1}{r}\frac{\partial}{\partial r}\left(r\frac{\partial u}{\partial r}\right)+\frac{1}{r^2}\frac{\partial^2 u}{\partial \theta^2}=\frac{1}{c^2}\frac{\partial^2 u}{\partial t^2} \tag{4}$$

converting it into a simpler form,

$$\frac{\partial^2 u}{\partial t^2}=c^2\left(\frac{\partial^2 u}{\partial r^2}+\frac{\partial u}{r\partial r^2}+\frac{\partial^2 u}{r^2\partial \theta^2}\right) \tag{5}$$

$$c=\sqrt{\frac{T}{\rho h}} \tag{6}$$

where, ρ is the membrane density and h is the membrane thickness.

Boundary Condition

The boundary conditions that were selected for the solution of the vibration modes for the circular membrane in polar coordinates were based on the model used by Nguyen et al. (2011). For a circular membrane fixed at the outer boundary, the deflection of the membrane at the radius of the membrane R (at $r = R$) is assumed to be zero; this implies that the membrane deflection decreases as the force approaches the edge of the circular boundary, expressed by the zeroing of the displacement variable, u:

$$u(R,t,\theta)=0 \tag{7}$$

To create a numerical solution for the vibration, the initial displacement of the membrane, $P(r,\theta)$, was set to zero and the membrane movement was triggered by an initial velocity, $Q(t)$. These conditions were expressed as:

$$P(r,\theta)=0 \quad \text{and} \quad Q(t)\neq 0 \tag{8}$$

Variable Separation

The displacement wave equation was legitimate under the condition of:

$$u=P(r,\theta)Q(t) \tag{9}$$

Embedding Equation 9 and its derivative in Equation 5, we derived:

$$\ddot{Q}P=c^2\left(\frac{\partial^2 P}{\partial r^2}Q(t)+\frac{\partial P}{r\partial r}Q(t)+\frac{\partial^2 P}{r^2\partial \theta^2}Q(t)\right) \tag{10}$$

reorganised by separation,

$$\frac{\ddot{Q}}{c^2 Q}=\frac{1}{P}\left(\frac{\partial^2 P}{\partial r^2}+\frac{\partial P}{r\partial r}+\frac{\partial^2 P}{r^2\partial \theta^2}\right) \tag{11}$$

Since both sides must be equal to a constant to generate a solution, a set of constants was drafted. Kreyszig (2011) introduced a negative constant ($-k^2$) to satisfy the boundary conditions without being zero, as given below:

$$\frac{\ddot{Q}}{c^2 Q} = \frac{1}{P}\left(\frac{\partial^2 P}{\partial r^2} + \frac{\partial P}{r\partial r} + \frac{\partial^2 P}{r^2 \partial \theta^2}\right) = -k^2 \tag{12}$$

$$\frac{\ddot{Q}}{c^2 Q} = -k^2 \tag{13}$$

$$\frac{1}{P}\left(\frac{\partial^2 P}{\partial r^2} + \frac{\partial P}{r\partial r} + \frac{\partial^2 P}{r^2 \partial \theta^2}\right) = -k^2 \tag{14}$$

Comparing Equation 13 and Equation 14 yielded the following two differential equations:

$$\ddot{Q} + \lambda^2 Q = 0 \tag{15}$$

where,

$$\lambda = ck \tag{16}$$

$$\frac{\partial^2 P}{\partial r^2} + \frac{\partial P}{r\partial r} + \frac{\partial^2 P}{r^2 \partial \theta^2} + k^2 P = 0 \tag{17}$$

Separating the variable, $P(r, \theta)$, by using the following equation in Equation 17, we derived:

$$P = V(r)W(\theta) \tag{18}$$

where, $V(r)$ is the variable for the radius of the membrane and $W(\theta)$ is the variable for the angle around the axis of the membrane. This gave us:

$$WV'' + \frac{1}{r}WV' + \frac{1}{r^2}VW'' + k^2 VW = 0 \tag{19}$$

which was simplified as:

$$W'' + W\frac{r^2 V'' + rV' + r^2 k^2 V}{V} = 0 \tag{20}$$

Allowing:

$$-\frac{W''}{W} = \frac{r^2 V'' + rV' + r^2 k^2 V}{V} = n^2 \tag{21}$$

resulted in the following expressions:

$$W'' + n^2 W = 0 \tag{22}$$

$$r^2 V'' + rV' + (k^2 r^2 - n^2)V = 0 \tag{23}$$

Allowing $s = kr$, then $\left({}^{k}/_{s}\right) = \left({}^{1}/_{r}\right)$ and ${}^{ds}/_{dr} = k$

$$\frac{dV}{dr} = \frac{dV}{ds}k \tag{24}$$

$$\frac{d^2V}{dr^2} = \frac{d^2V}{ds^2}k^2 \tag{25}$$

Using Equation 24 and 25 in Equation 23 gave us the following:

$$\frac{d^2V}{ds^2}k^2 + \frac{1}{r}\frac{dV}{ds}k + \left(k^2 - \frac{n^2}{r^2}\right)V = 0 \tag{26}$$

Substituting $r = {}^{s}/_{k}$, we got:

$$\frac{d^2V}{ds^2} + \frac{1}{s}\frac{dV}{ds} + \left(1 - \frac{n^2}{k^2r^2}\right)V = 0 \tag{27}$$

This is Bessel's equation, as given in mathematical literature (Fletcher & Rossing, 1998). The solution of Bessel's equation was:

$$V_n(r) = J_n(s) = J_n(kr) \tag{28}$$

Equation 22 was also solved in the following method (Kreyszig, 2011):

$$W_n = \cos(n\theta) \;\; for \;\; n = 0,1,2, \ldots \tag{29}$$

Thus, using Equation 10:

$$P = J_n(kr)\cos(n\theta) \tag{30}$$

and using Equation 9:

$$u(r,t,\theta) = P(r,\theta)Q(t) = J_n(kr)\cos(n\theta)\,Q(t) \tag{31}$$

where the Eigen function $Q(t)$ can be expressed by the Fourier series as follows (Soedel, 2004):

$$Q_{mn}(t) = a_{mn}\cos(ck_{mn}t) + b_{mn}(ck_{mn}t) \;\; for \;\; m = 0,1,2, \ldots \tag{32}$$

Thus, Equation 30 can be rewritten as:

$$u_{mn}(r,t,\theta) = [a_{mn}\cos(ck_{mn}t) + b_{mn}sin(ck_{mn}t)]J_n(k_{mn}r)cos(n\theta) \tag{33}$$

Since, $u(R,t,\theta) = 0$

$$k_{mn} = {\alpha_{mn}}/{R} \tag{34}$$

α_{mn}= number of roots

The Fourier series coefficients are, therefore:

$$a_{mn} = \frac{2}{R^2 J_1^2(\alpha_{mn})} \int_0^R rp(r) J_0\left(\frac{\alpha_{mn}}{R} r\right) dr \tag{35}$$

$$b_{mn} = \frac{2}{c\alpha_{mn} R J_1^2(\alpha_{mn})} \int_0^R rq(r) J_0\left(\frac{\alpha_{mn}}{R} r\right) dr \tag{36}$$

and initial displacement and initial velocity are as follows, respectively:

$$p(r) = u(r,0) \; and \; q(r) = \left.\frac{\partial u}{\partial t}\right|_{t=0} \tag{37}$$

The "α_{mn}" is defined as the *mth* positive zeros of $J_n(s)$, where m represents the nodal circle and n represents the nodal line. The positive zeros can be determined by plotting the zero-th order of the Bessel function as shown in Table 1, as found in Baricz (2010).

Table 1
Values for α_{mn}

	n			
m	1	2	3	4
0	2.4048	5.520	8.654	11.792
1	3.832	7.016	10.173	13.323
2	5.135	8.417	11.620	14.796
3	6.379	9.760	13.017	16.224

Natural Frequency

Using Equation 6 and 34 in Equation 16 provided the frequency of the membrane:

$$\lambda_{mn} = \frac{\alpha_{mn}}{R}\sqrt{\frac{T}{\rho h}} \tag{38}$$

RESULTS AND DISCUSSION

A numerical example for the first three vibrational modes where m=0 and n=1 until m=0 and n=3 is illustrated in this paper. Numerical calculation from the mathematical formula was conducted using the Smath software. The Smath software was utilised to calculate the numerical

example and to illustrate the result generated from the functions. The portrayed result in the Smath software was the value evaluated from Equation 32 for simulated 3D images of mode 01, mode 02 and mode 03, while Equation 39 provided the natural frequency, respectively. The result derived using the Smath software was then validated using the finite element analysis software, Mecway, to ensure the numerical result formulated in the Smath was correct and to determine the percentage error. For the finite element analysis in Mecway, 256 quad 8 elements were administrated with a total of 833 nodes for each of the modes simulated. The value of error between the two methods was later documented for further analysis and discussion.

The real *kompang* numeral cases were used as an example, with the radius of the circular membrane, R, given as 0.25m. Using the Hot Tack Tester V2.04.1 (see Figure 4), the tension of the membrane was determined to be about 100 N per length, which was proven to be within the range of the value provided by Salehi et al. (2014) and was assumed to be constant across both types of skin. The density of both types of skin was determined using $\rho = \frac{m}{v}$; this gave the goat-skin density as 552.905 $^{kg}/_{m^3}$ and that of the x-ray film as 1402.56 $^{kg}/_{m^3}$, therefore automatically generating the *c* value of 0.6014 $^{Nm^2}/_{kg}$ for the goat skin and 0.3776 $^{Nm^2}/_{kg}$ for the x-ray film.



Figure 4. The Hot Tack Tester V2.04.1 was used for determining the tension limit of the two types of membrane

The Fourier series with initial velocity of 0.5 $^{m}/_{s}$ and initial deflection of zero coefficients were then determined. A suitable initial boundary condition was important for an accurate result (Torin & Bilbao, 2013). By using these values in Equation 25 for 3D portrayal of the mode states and Equation 32 for natural frequency in the Smath software, we derived the vibrational deflection modes for mode 01, mode 02 and mode 03 with their natural frequency, as shown in Figure 4 using goat skin and Figure 5 using x-ray film membrane for the two types of *kompang*.

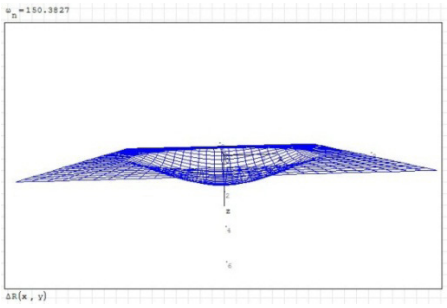

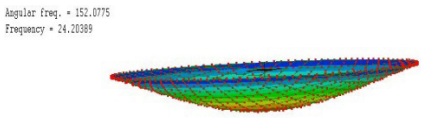

ω_{01}=150.3827 ω_{01}=152.0775

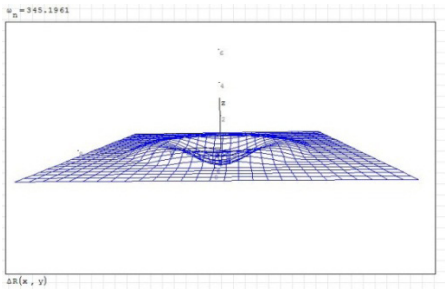

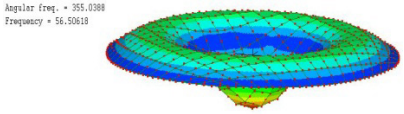

ω_{02}=345.1961 ω_{02}=355.0388

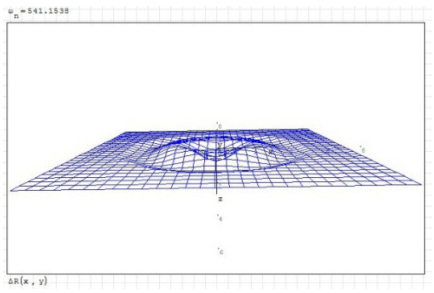

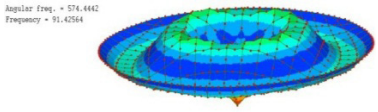

ω_{03}=541.1538 ω_{03}=574.4442

Figure 5. Results of mode 01, mode 02 and mode 03 of goat-skin *kompang* simulated in the Smath (left) and Mecway software (right)

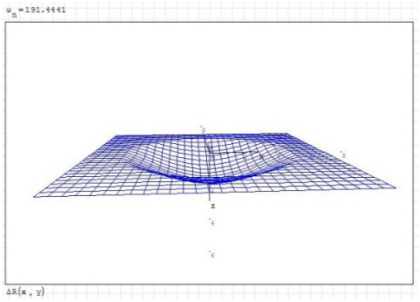

ω 01=191.4441

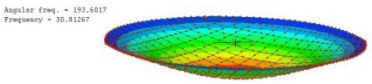

ω 01=193.6017

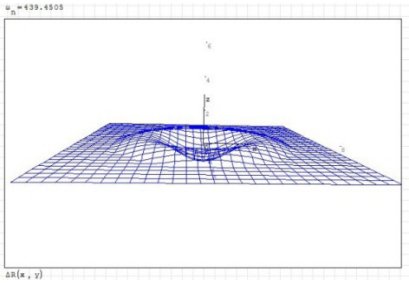

ω 02=439.4505

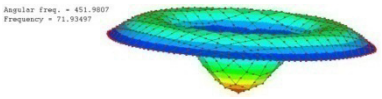

ω 02=451.9807

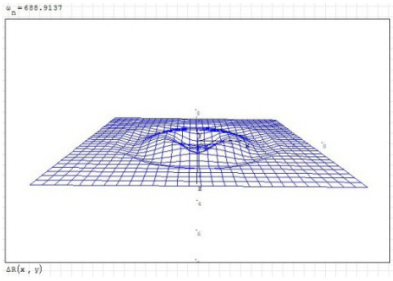

ω 03=688.9137

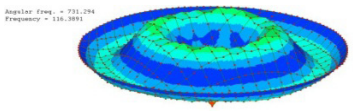

ω 03=731.294

Figure 6. Results of mode 01, mode 02 and mode 03 of X-ray film *kompang* simulated in the Smath (left) and Mecway software (right)

Figure 5 and Figure 6 show the results of mode 01, mode 02 and mode 03 generated by use of the *kompang* using the numerical calculation approach provided by Smath and finite element analysis provided by Mecway for the two types of *kompang* membrane. Figure 5 shows the natural frequency results for the goat-skin membrane derived from the numerical calculation in the Smath software: 150.3827 $^{rad}/_{sec}$ for mode 01, 345.1961 $^{rad}/_{sec}$ for mode 02 and 541.1358 $^{rad}/_{sec}$ for mode 03. Using Mecway provided these results: 152.0775 $^{rad}/_{sec}$ for mode 01, 355.0388 $^{rad}/_{sec}$ for mode 02 and 574.4442 $^{rad}/_{sec}$ for mode 03.

Figure 6 shows the results collected for the x-ray-film *kompang*: the natural frequency value obtained was 191.4441 $^{rad}/_{sec}$ for mode 01, 439.4505 $^{rad}/_{sec}$ for mode 02 and 688.9137 $^{rad}/_{sec}$ for mode 03 in numerical calculation in Smath. Meanwhile, the finite element analysis using Mecway showed these results: 193.6017 $^{rad}/_{sec}$ for mode 01, 451.9807 $^{rad}/_{sec}$ for mode 02 and 731.294 $^{rad}/_{sec}$ for mode 03. These results implied that the x-ray-film *kompang* produced a slightly higher natural frequency compared with the goat-skin *kompang*. This finding was supported by the findings of Christopher and Umesh (2006), who reported that in percussion musical instruments, the higher density of the membrane results in a higher value for the natural frequency.

Percentage Error

To calculate the percentage error of value between the values generated by the Smath and Mecway software, we used mode 01 for the goat-skin membrane *kompang* as an example, as given below:

$$\frac{|approximate\ value - exact\ value|}{|exact\ value|} \times 100\% \tag{33}$$

$$\frac{|150.3827 - 152.0775|}{|152.0775|} \times 100\%$$

$$= 1.11\%$$

Table 2
Percentage error of frequency surveyed between smath and mecway software results for goat skin membrane

Mode	Goat Skin		Percentage Error (%)
	Smath	Mecway	
01	150.3827	152.0775	1.11
02	345.1961	355.0388	2.77
03	541.1538	574.4442	5.79

Table 3
Percentage error of frequency surveyed between smath and mecway software results for x-ray-film membrane

Mode	X-Ray Film		Percentage Error (%)
	Smath	Mecway	
01	191.4441	193.6017	1.11
02	439.4505	451.9807	2.77
03	688.9137	731.294	5.79

Table 2 and Table 3 shows the summarised results obtained from using the numerical mathematical calculation generated by Smath and the finite element analysis method using Mecway for both types of skin. Table 2 and Table 3 show that the frequency increased dramatically from mode 01 to mode 02 and from mode 02 to mode 03.

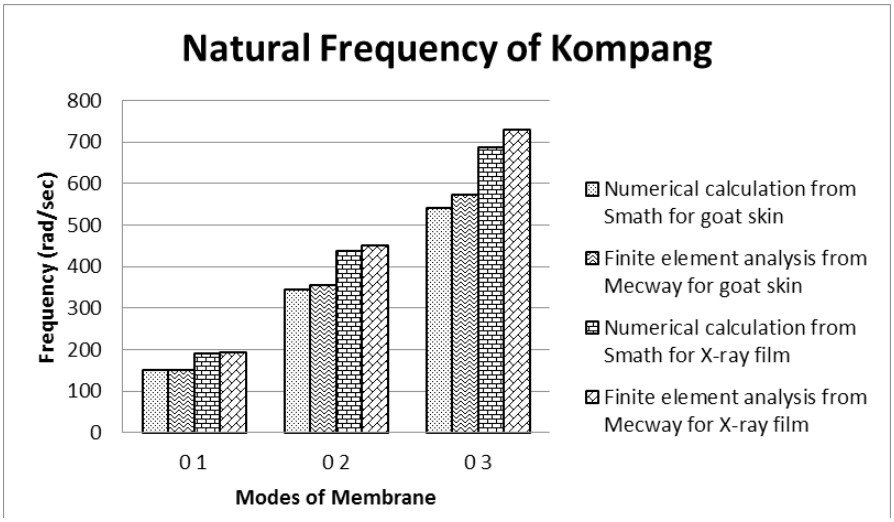

Figure 7. Chart representing the evaluated results obtained from the numerical calculation using Smath software and finite element analysis using Mecway software

Figure 7 shows the chart generated for both types of *kompang* in terms of natural frequency content with respect to mode 01, mode 02 and mode 03. From the graph plotted, it was found that the reading generated from Smath software almost overlapped the reading provided by Mecway software for mode 01 and the gap, which showed that the error widened as it proceeded from mode 02 to mode 03.

The increase in percentage error from mode 01 to mode 03 shown by the Mecway software compared with the results from the Smath software was probably due to the limited number of nodes, causing the movement to be less smooth in mode 02 and mode 03 compared with in mode 01 (refer to Figure 5 and Figure 6). Increasing the number of nodes allowed the results to be closer to the values generated by Smath since in finite element analysis, the more the number of nodes installed, the better the results obtained (Dow, 1998).

Despite this, the value of error ranging from 1.11% to 5.79% is considered to be a small error and therefore, can be neglected. This result demonstrated that the mathematical approach of Smath provided for more accurate results and was suitable for evaluating the musical instrument, the *kompang*.

CONCLUSION

To analyse the use of the type of membrane used in the traditional percussion instrument, the *kompang*, the Fourier-Bessel solution for the circular membrane vibration modes shown in this paper was used by utilising the wave equation in polar coordinates. The developed vibration modes were based on Bessel functions, with solution derivatives from the Fourier series. The solutions in the Smath were a purely mathematical approach to vibrational normal mode development using polar coordinates. The value for natural frequency provided by mathematical calculation derived from Smath were proved to be almost similar to the results generated by finite element analysis in Mecway, with a very small error, hinting that the mathematical approach was suitable and relevant for analysing the musical instrument, the *kompang*.

ACKNOWLEDGEMENT

The authors acknowledge the financial support provided by the Malaysian Ministry of Education and Universiti Tun Hussein Onn Malaysia (Fundamental Research Grant Scheme vot. 1206).

REFERENCES

Abdullah, M. H. (2005). *Kompang: An organological and ethnomusicological study of a Malay frame drum.* (Master Thesis). Newcastle University, UK.

Bank, B., & Sujbert, L. (2006). *Physics-based sound synthesis of stringed instruments including geometric nonlinearities*. (PhD Thesis). Budapest University of Technology and Economics, Hungary.

Baricz, A. (2010). *Generalized Bessel functions of the first kind.* New York, NY: Springer.

Bertsch, M. (2001). Vibration patterns and sound analysis of the Viennese Timpani. In *Proceedings of ISMA* (pp. 1-4). Perugia, Italy.

Bilbao, S. (2012). Time domain simulation and sound synthesis for the snare drum. *The Journal of Acoustical Society of America, 131*(1), 914–925.

Bilbao, S., & Webb, C. (2012). Timpani drum synthesis in 3D on GPGPUs. In *Proceedings of the 15th International Conference on Digital Audio Effects (DAFx-12)* (pp. 1-8). York, United Kingdom.

Christian, R. S, Davis, R. E., Tubis, A., Anderson, C. A., Mills, R. I., & Rossing, T. D. (1984). Effects of air loading on timpani membrane vibrations. *The Journal of Acoustical Society of America*, *76*(5), 1336–1345.

Christopher, H. M. J., & Umesh, A. K. (2006). Membrane vibration experiments: An historical review and recent results. *The Journal of Sound and Vibration, 295*(3), 602–613.

Dow, J. A. T. (1998). *A unified approach to the finite element method and error analysis procedures.* United States of America, USA: Academic Press.

Fletcher, N. H., & Rossing, T. (1998). *The physics of musical instruments.* New York: Springer-Verlag.

Ismail, A., Samad, S. A., Hussain, A., Azhari, C. H., & Zainal, M. R. M. (2006). Analysis of the sound of the kompang for computer music synthesis, SCOReD 2006. In *Proceedings of 2006 4th Student Conference on Research and Development "Towards Enhancing Research Excellence in the Region* (pp 95–98). IEEE.

Karjalainen, M., Backman, J., & Polkki, J. (1993). Analysis, modeling, and real-time sound synthesis of the kantele, a traditional Finnish string instrument. In *Proceedings of the 1993 IEEE International Conference on Acoustics, Speech, and Signal Processing: Plenary, Special, Audio, Underwater Acoustics, VLSI, Neural Networks – Volume I* (pp. 229–232). Washington, DC: IEEE Computer Society.

Kreyszig, E. (2011). *Advanced engineering mathematics.* United States of America, USA: Jhon Wiley & Sons.

Morse, P. M. (1948). *Vibration and sound.* New York, NY: McGraw-Hill.

Nguyen, D. M., Anton, E., Allan, R. G., & Jens, G. (2011). Isogeometric shape optimization of vibrating membranes. *Journal of Computer Methods in Applied Mechanics and Engineering, 200*(13), 1343–1353.

Ono, T., Takahashi, I., Takasu, Y., Miura, Y., & Watanabe, U. (2009). Acoustic characteristics of Wadaiko (traditional Japanese drum) with wood plastic shell. *The Journal of Acoustical Science and Technology, 30*(6), 410–416.

Rhaouti, L., Chaigne, A., & Joly, P. (1999). Time-domain modeling and numerical simulation of a kettledrum. *The Journal of Acoustical Society of America, 105*(6), 3545–3562.

Rossing, T. D., Bork, I., Zhao, H., & Fystrom, D. O. (1992). Acoustics of snare drums. *The Journal of Acoustical Society of America, 92*(1), 84–94.

Salehi, M., Kadim, I., Mahgoub, O., Negahdari, Sh., & Naeeni, R. S. E. (2014). Effects of type, sex and age on goat skin and leather characteristics. *The Journal of Animal Production Science, 54*(5), 638–644.

Siswanto, W. A., Che Wahab, W. M. A., Yahya, M. N., Ismail, A. E., Nawi, I. (2014). A platform for digital reproduction sound of traditional musical instrument kompang. *Applied Mechanics and Materials, 660,* 823–827.

Soedel, W. (2004). *Vibrations of shells and plates* (3rd Ed.). United States of America, USA: CRC Press.

Torin, A., & Bilbao, S. (2013). Numerical experiments with non-linear double membrane drums. In *Proceedings of the Stockholm Musical Acoustics Conference/Sound and Music Computing Conference* (pp. 569-576). Stockholm, Sweden.